Growth of Multiple-Site Fatigue Damage (MSD) in an Undamaged Fuselage Lap Joint Curved Panel

Abubaker A. Ahmed
FAA-Drexel Fellow, Mechanical Engineering and Mechanics Department, Drexel University

John G. Bakuckas, Jr. and Paul W. Tan, AAR-450
FAA William J. Hughes Technical Center, Atlantic City International Airport, NJ

Jonathan Awerbuch, Alan C. Lau, and Tein-Min Tan
Faculty, Department of Mechanical Engineering and Mechanics, Drexel University

Abstract

This paper presents the results of experimental and computational investigations on the initiation, growth, and interaction of multiple-site damage (MSD) in an initially pristine fuselage lap joint curved panel subjected to fatigue loading. The panel was tested at the Full-Scale Aircraft Structural Test Evaluation and Research facility at the Federal Aviation Administration William J. Hughes Technical Center. A constant-amplitude load spectrum with underload marker cycles was used in the fatigue test to enable fractographic analysis of the crack surfaces. MSD cracks were observed emanating from rivet holes in the lap joint area. Crack linkup occurred in the outermost fastener row in the lap joint. Results show that the majority of fatigue life was spent in initiating individual multiple-site cracks. After the linkup of MSD cracks from two adjacent rivet holes, crack growth rates increased substantially. Computational simulations of the damage growth were conducted using probabilistic fatigue crack growth models and finite element analyses. Simulation results compared well with the experimental observations. A residual strength test was conducted with the panel being loaded quasi-statically until it failed catastrophically.

Introduction

Multiple-site damage (MSD) is a source of widespread fatigue damage (WFD) that is characterized by the simultaneous presence of fatigue cracks in the same structural element [1]. Riveted airframe joints are susceptible to MSD cracks, especially in aging transport aircraft. Previous studies were conducted on fuselage panels at the Full-Scale Aircraft Structural Test Evaluation and Research (FASTER) facility at the Federal Aviation Administration (FAA) Technical Center to examine the effects of multiple cracks on the fatigue crack growth and residual strength of large lead cracks. Panels with two different joint configurations, longitudinal lap joints and circumferential butt joints, were tested. Initial damage scenarios were inserted into the joints as either a lead crack only or a lead crack and multiple small cracks ahead of it. Results from those studies showed that the presence of MSD reduced the number of cycles to grow the lead crack to the final length by approximately 37%. The load-carrying capacity of the panels was also reduced by about 20% as a result of the presence of MSD [2].

The primary focus of this study is on the MSD initiation, evolution, and interaction in a pristine fuselage panel subjected to a fatigue loading. The test panel contains a longitudinal lap joint with four rows of countersunk rivets. A constant-amplitude fatigue loading simulating the fuselage cabin pressurization condition was applied using the FASTER test fixture. A quasi-static test was conducted prior to the fatigue test to ensure proper load introduction to the panel and to validate a finite element model of the panel. MSD crack formation and linkup were monitored and recorded using the Self-Nulling Rotating Eddy-Current Probe system and the Remote-Controlled Crack Monitoring (RCCM) system. The fatigue test was terminated after observing the rapid growth of the lead crack, and then the panel was loaded quasi-statically up to final failure to measure the residual strength. A probabilistic analysis using an existing risk assessment code was conducted to predict the first linkup of MSD cracks.

Stress-intensity factors for the state of damage after crack linkup were calculated with a geometrically nonlinear finite element analysis. Results presented in this paper show incident-by-incident details of the formation and interaction of MSD cracks, residual strength characteristics of the panel, as well as probabilistic and finite element analysis results.

Test Facility

As part of The National Aging Aircraft Research Program, the FASTER facility was established at the FAA William J. Hughes Technical Center for testing large curved panels representative of aircraft fuselage structures. The FASTER facility provides experimental data to validate and support analytical methods under development, including WFD prediction, repair analysis and design, and new aircraft design methodologies. The facility hosts a test fixture that is capable of applying to full-scale curved panels a combination of loads, including internal pressurization, tensile hoop, longitudinal, and frame loads, and skin shear loads, that simulates real flight loading conditions encountered by an aircraft fuselage. Both quasi-static and long-term durability spectrum loadings can be applied in the FASTER facility. A detailed description of the FASTER facility and test fixture can be found in reference 2.

Two crack inspection methods, the Self-Nulling Rotating Eddy-Current Probe system and the RCCM system, have been used to detect and monitor crack formation and propagation. The rotating probe system is capable of detecting cracks that are hidden underneath countersunk rivet heads without removing the fastener. It has a 90% probability of detecting a hidden crack of 0.032″ in size [3]. The RCCM system is a video data acquisition system consisting of two computer-controlled, high-precision x-y-z translation stages, each instrumented with a wide-field-of-view camera and a narrow-field-of-view camera. The combination of the two cameras allows monitoring the entire panel surface at several levels of magnification providing a field of view ranging from 0.05″ up to 14″. Each translation stage has a motion resolution of 0.00039″ (1 μm) allowing an accurate tracking of crack growth [2].

Panel Configuration

The pristine curved panel used in the test (Figure 1) is 120″ by 68″ with a radius of 66″. It was manufactured per airframe manufacturers specifications and is representative of a narrow-body fuselage structure. Substructure of the panel includes six frames extending in the circumferential direction with a 19″ spacing and seven stringers in the longitudinal direction with a 7.5″ spacing. The skin thickness is 0.063″. Both the skin and substructure are made of 2024-T3 aluminum. A longitudinal lap joint with two skin layers and two finger doubler layers is located in the middle of the panel along stringer S4. The lap joint contains four rivet rows, labeled A, B, C, and D, respectively, as shown in Figure 1. The four edges of the panel were reinforced with aluminum doublers; holes were placed along the doublers so that the hoop and longitudinal load assemblies can be attached to the panel. The two ends of each frame, where the frame load assemblies are attached, were also reinforced with aluminum doublers. An elastomeric seal was bonded along the perimeter of the inner surface of the curved panel to attach to the pressure box of the FASTER fixture.

The test panel was fully instrumented with strain gages to monitor and record strain distribution during the test. Strain gages were installed on the skin, frames, and stringers. Several back-to-back strain gage sets were installed at various locations on the skin to measure out-of-plane bending deformation. After MSD cracks developed and linked up to form a lead crack, additional strain gages were installed near the rivet holes ahead of the lead crack to monitor the local damage effect on the strain behavior.

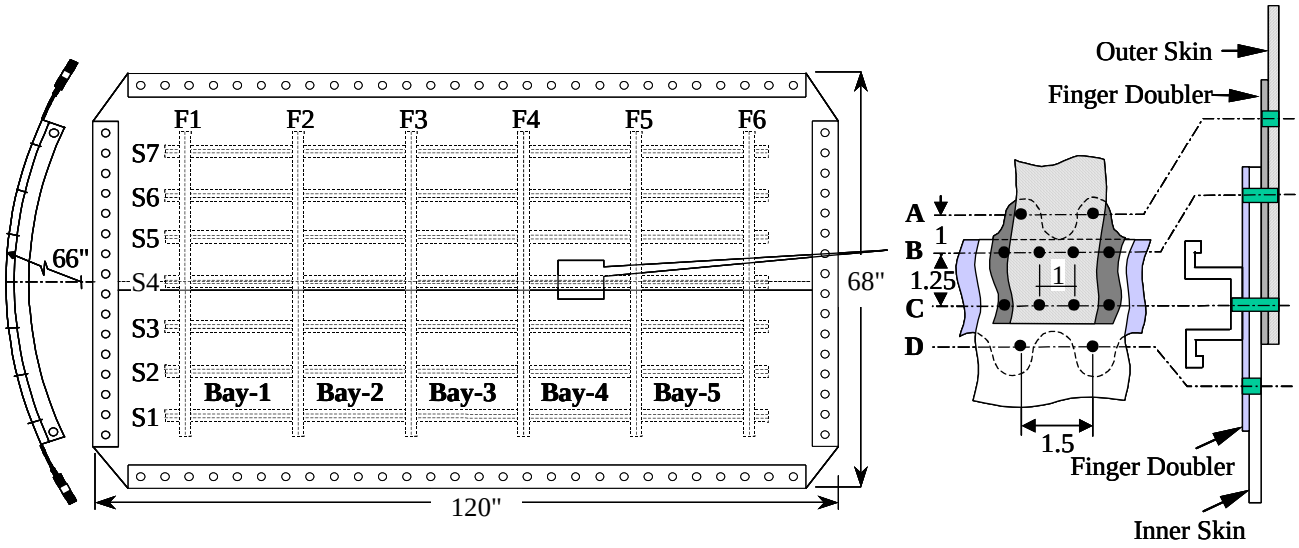

Figure 1. Test panel dimensions and lap joint configurations.

Test Procedure

The test was conducted in three phases with the loading conditions shown in Table 1. Loads representative of a cabin pressurization condition, including internal pressure, tensile skin loads in the hoop and longitudinal directions, and tensile frame loads in the hoop direction, were applied to the panel. To accelerate the test, the maximum applied loads were higher than the typical operational loads of a fuselage structure. In phase I, prior to the fatigue loading, loads were applied quasi-statically to ensure proper load transfer from the fixture to the test panel. Strains were measured and recorded at all strain gages and the strain distribution was studied to identify critical locations in the panel. The strain gage measurements were also used to validate a finite element model of the test panel.

Phase II, the fatigue test, was conducted using a constant-amplitude load spectrum with underload cycles having amplitude of 75% of the maximum load. The purpose of using underload cycles is to mark the fracture surfaces so that a fractographic study can be conducted after the completion of the test to reconstruct and map the crack growth histories. MSD cracks were detected at the upper skin shear clip rivet holes near the lap joint and in the lap joint outer rivet row. The fatigue test was terminated after several crack linkups had occurred and the crack grew rapidly.

Residual strength of the damaged panel was investigated in phase III of the test by loading quasi-statically to failure. The internal pressure applied to the panel was increased in a 2-psi increment up to 14 psi, and with a 1-psi increment thereafter. Strain gage measurements and crack lengths were recorded continuously throughout the residual strength test.

Table 1. Test phases and applied loads.

Test Phase	Purpose	Load Type	Maximum Loads			
			Pressure, psi	Hoop, lb/in	Frame, lb/in	Long., lb/in
I	Strain Survey	Quasi-Static	16.0	878.6	177.4	528.0
II	Fatigue crack growth	Cyclic, R=0.1	16.0	878.6	177.4	528.0
III	Residual Strength	Quasi-Static	Loads incremented up to catastrophic failure			

Finite Element Analysis

A finite element (FE) model of the pristine curved panel was developed to conduct geometrically nonlinear analyses to simulate the tests. The skin and substructure were modeled using shell elements. Rivets were modeled with three-dimensional linear beam elements. Distributed load was applied to the inner surfaces of the model to simulate the internal pressure. Hoop, longitudinal, and frame loads were simulated using nodal point forces. Strain measurements from the test panel were used to validate the finite element model by comparing the test data to the analysis predictions. Details of the model are in reference 4. The FE model was modified later to include the lead crack formed by the first MSD linkup. The modified crack closure integral method was applied to determine the stress-intensity factors [2] for the mixed-mode crack growth.

Probabilistic Crack Growth Simulations

A probabilistic risk assessment code, TRACLIFE, was used to predict the number of fatigue cycles to the first linkup in the curved panel [5]. First linkup was predicted at 107,250 fatigue cycles with a 99% probability. That number of cycles was within 1% of the actual cycles to linkup. In TRACLIFE predictions, results from a FAA-USAF study on flat panel [6] with similar lap joint configuration to the curved test panel were used to establish the equivalent initial flaw size (EIFS). Initially, three-dimensional crack growth analysis was conducted until the cracks propagated through the skin thickness. Subsequently, two-dimensional analysis was adopted for the through-thickness cracks. The Paris law, with constants obtained by curve-fitting the flat panel results, was used to calculate crack growth. The Random Sampling Condensation Algorithm with various probabilistic sample sizes was applied to model random variations in parameters such as EIFS, the Paris law constants, and the fracture toughness. Additional TRACLIFE analyses were conducted in this study to predict crack growth behavior of individual MSD cracks prior to the first linkup.

Results and Discussion

Phase I, Strain Survey

Strain distributions in the panel were recorded under the quasi-static loading condition described in Table 1. Results compared well with the results of a full-scale verification test conducted on an aft fuselage section of a narrow-body aircraft. This confirmed proper load transfer into the panel from the FASTER test fixture [4].

The eccentricity in the loading path due to the lap joint geometry produces severe out-of-plane bending deformation in the lap joint area. Several sets of back-to-back strain gages were installed at various locations on the panel to verify this local bending effect. Figure 2 depicts schematically the locations of four such back-to-back gage sets: (1) set 33/34 at a skin mid-bay region, (2) set 38/38B at a distance of 0.5″ above rivet row A, (3) set 39/39B along rivet row A midway between two rivets, and (4) set 45/45B 0.5″ below rivet row D. The membrane strain component (the average of the strain measurements at the inner and outer surfaces) and bending strain component (half of the difference between the two measurements) for each gage set are shown in Figure 2. It can be seen that the membrane strain component is nearly the same at the four locations. The bending strain component, on the other hand, differs significantly, with the highest value being recorded at gage set 39/39B along rivet row A. As a result of this severe local bending, the skin inner surface along the outer rivet row of the lap joint experiences high tensile stresses making this rivet row a critical area for damage initiation. Local bending also explains why cracks generally initiate at the skin inner-faying surface and propagate outward.

Figure 2 also shows the predictions of the geometrically nonlinear finite element analyses. It can be seen that the predictions of membrane strain components compare very well with the strain gage measurements. Predictions of the bending strain component in the lap joint region, on the other hand, are not as good and are in general lower than the strain gage measurements. In the finite element model,

rivets in the lap joint region are represented by beam elements, and a perfect bonding between rivets and skins assumed. These assumptions make the finite element model much stiffer than the actual structure, resulting in lower strain values in the lap joint region.

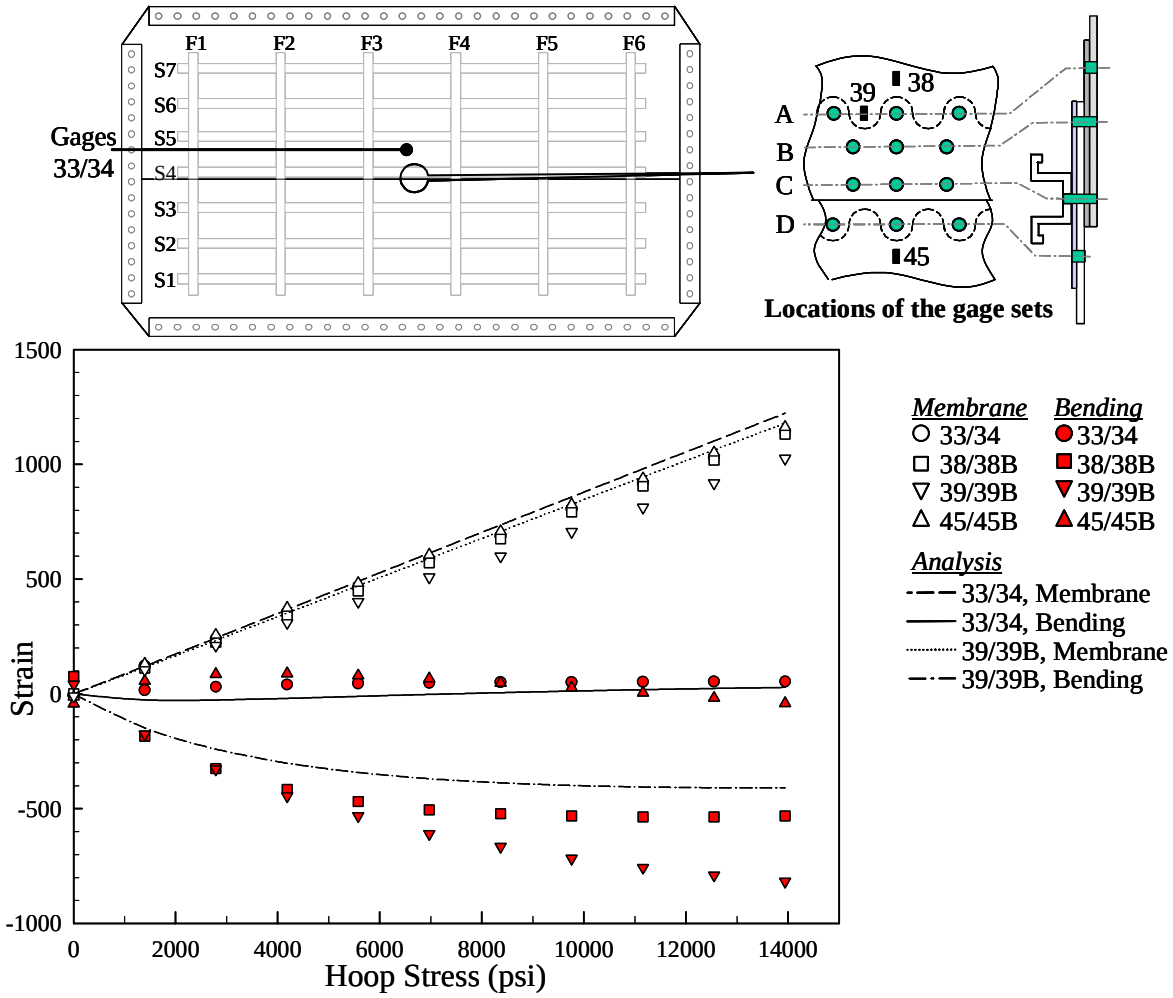

Figure 2. Membrane and bending strain components at four back-to-back strain gage locations on the skin.

Phase II, Fatigue Test

(a) Eddy-Current Inspections

Figure 3 shows the output of the Self-Nulling Rotating Eddy-Current Probe system obtained from the rivet hole of rivet A23. Output amplitudes above the threshold (15 mV) indicate presence of damage. Results in Figure 3 show that high eddy-current signals were detected at the +120º and -120º locations, indicating possible existence of hidden cracks. Figure 4 schematically depicts the evolution of the distribution of rivets in the lap joint area showing high eddy-current signal during the test. After 26,360 fatigue cycles, high eddy-current signal was detected at 3% of the rivets in row A and four rivets in row B. After 53,470 cycles, 11% of row-A rivets exhibited high signals while the number of high-signal rivets in row B remained unchanged. After 75,114 fatigue cycles, 20% of row-A rivets and 4 out of the 6 shear clip rivets near row A showed high eddy-current signal. At 107,222 cycles, shortly before the end of the fatigue test, 48% of row-A rivets and all but one shear clip rivets near row A had high eddy-current

signal. By that time, visual damage has been detected at those shear clip rivets and in row A and several crack linkups have occurred.

MSD cracks in the panel were detected only at rivet holes in row A and at the nearby shear clip rivet holes. Although indications of subsurface damage were seen in rows B and C, no visual cracks were detected in those rivet rows. Some row-B rivets have shown high signal since the baseline inspection, but no visible cracks. Rivet row D was not accessible for inspection with the rotating probe system during the test. Through a special setup, rivets in row D were inspected at the end of the fatigue test and high signals were found at three rivets. The fact that most damage indications were found in the lap joint outer rivet row can be attributed to the significant out-of-plane deformation of the skin along that rivet row as was indicated by the results of test phase I.

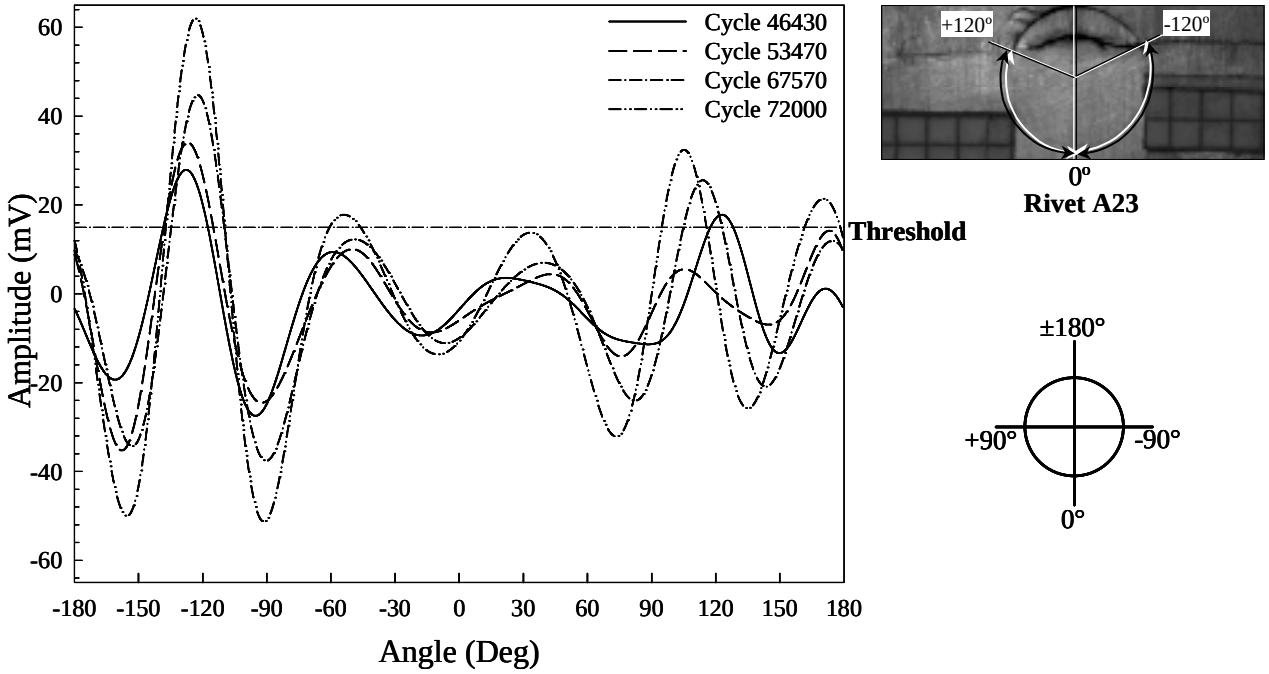

Figure 3. Eddy-current inspection results of rivet A23 showing signal amplitude vs angular location.

The rotating probe was very effective in qualitatively locating subsurface damage. Consequently, all cracks were anticipated before they became visible. Eddy-current signals may be correlated to crack sizes by using a lap joint specimen having cracks of known sizes. Future fractographic analysis of rivet holes with high eddy-current signal may establish correlation between eddy-current signal signatures and the fracture features.

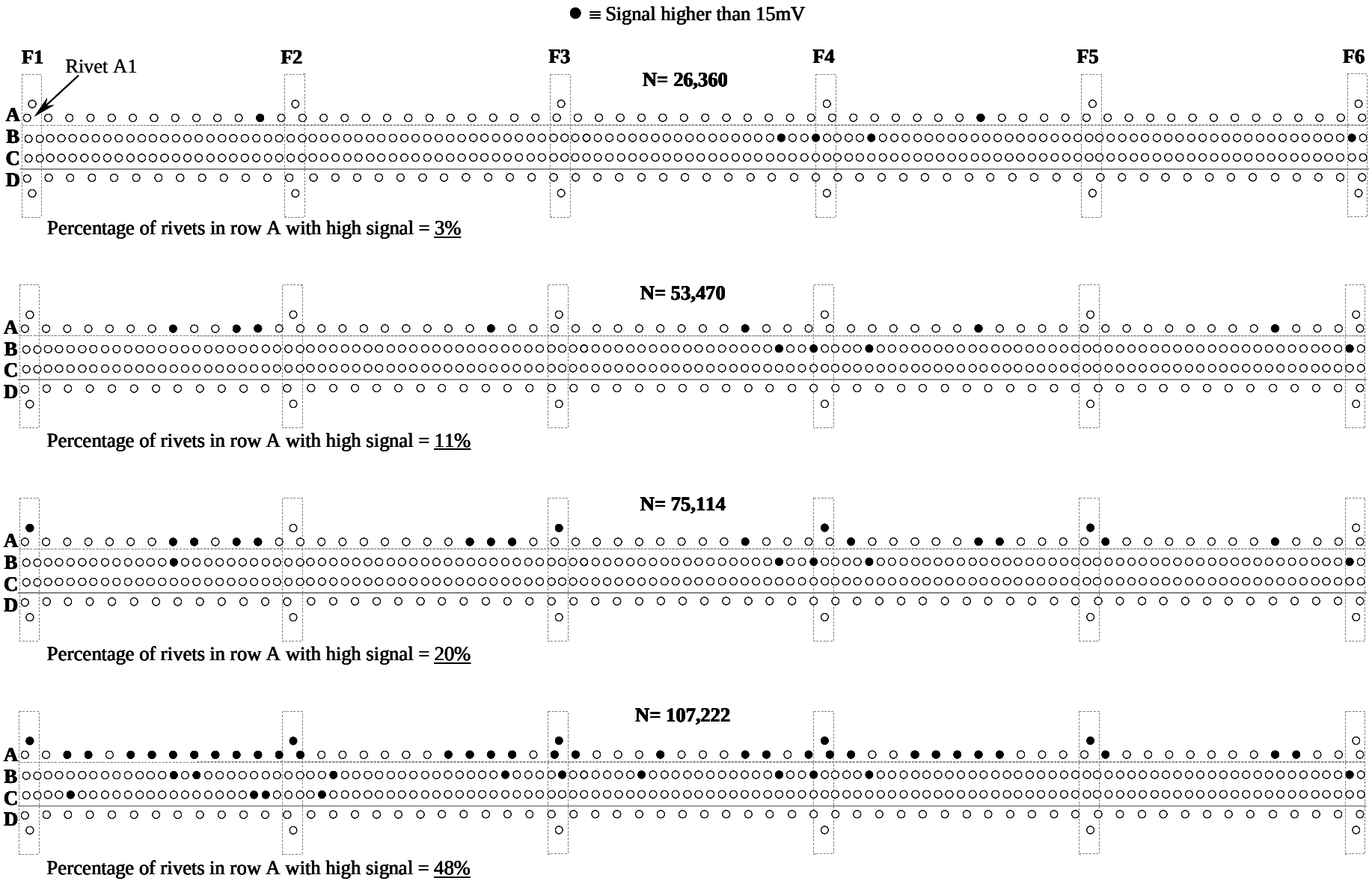

Figure 4. Locations of rivets with high eddy-current signal at different stages of the fatigue test.

(b) MSD Evolution

Visible MSD cracks were detected in two areas in the panel: the lap joint outer rivet row and the nearby outer skin shear clip rivet locations. MSD cracks initially formed both on the rivet heads and in the skin. After 51,500 full-load cycles, a curved crack in the rivet head was detected in rivet A23 located between frames 2 and 3 (Figure 5(a)). Similar rivet head cracks were detected at seven other rivets in row A. Water leakage from the rivet head cracks indicated that the cracks were through the thickness. Apparently, the high out-of-plane bending along rivet row A (see test phase I) caused the skin to push up against the rivet heads to form the cracks (Figure 5). Since the panel was constructed per the original equipment manufacturer specifications, the rivets were not designed to sustain loads as high as was applied in the fatigue test. Future fractographic analysis may define the mechanism of formation of these rivet head cracks.

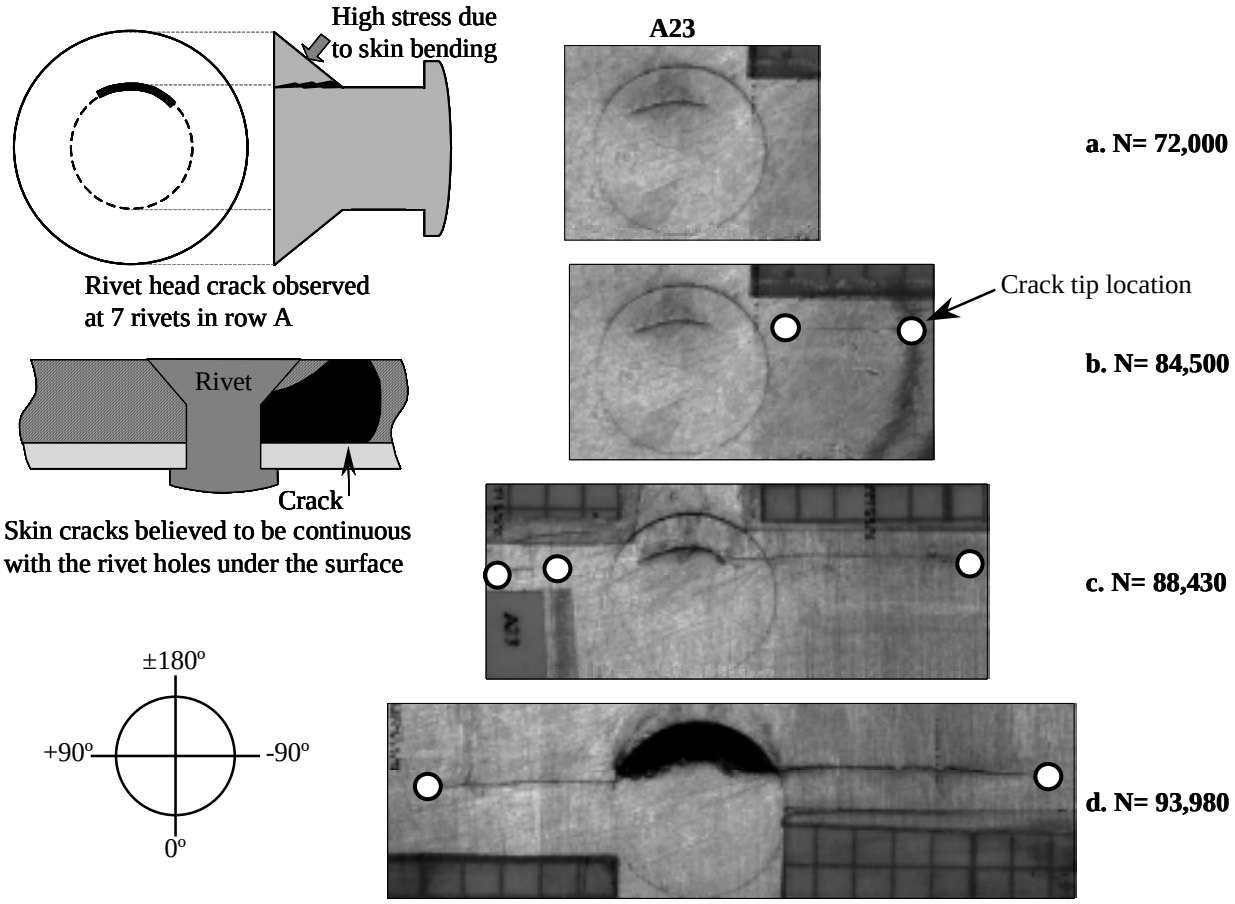

Figure 5. Damage evolution at rivet A23 of the lap joint outer rivet row. The white circles indicate crack tip locations.

Cracks in the skin of the lap joint were detected near rivet A23 in the outer rivet row (Figure 5). The first crack, designated crack A23R, was detected at about -120° orientation after 80,550 fatigue cycles. This crack initiated at a distance from the edge of the rivet hole and grew to linkup to the rivet hole (Figure 5(b)). Later, crack A23L was detected on the other side (left side) of rivet A23 at about

+120° orientation (Figure 5(c)). This crack also initiated at a distance from the rivet hole and linked up to the rivet hole.

The rivet-head crack of rivet A23 grew across the rivet head and linked with the skin cracks on both sides of the rivet. The upper portion of the rivet head was completely separated (Figure 5(d)). Two skin cracks, A22L and A22R, were later detected at the neighboring rivet A22. The two cracks at rivet A22 also initiated at away from the rivet hole. It appears that the cracks at rivets A22 and A23 had completely linked up to the rivet hole below the surface by the time they were detected on the surface (Figure 5). It is possible that residual stresses from the riveting process may have caused the cracks to propagate to the surface away from the rivet holes. Future analysis and fractographic examination will provide information on this phenomenon.

Visible MSD cracks were also detected emanating from the shear clip rivet holes near the outer rivet row of the lap joint. Those rivet holes are 0.84″ away from rivet row A. Figure 6 depicts RCCM images of the skin cracks at rivet F5-5 at frame 5. The first crack at that rivet was detected at and orientation of -90° after 75,510 full-load fatigue cycles. A second crack was detected 50 fatigue cycles later at +15° orientation. At 76,630 cycles, a third crack was detected at rivet F5-5 at +45° location. More cracks were detected at the same time at rivets F4-5 at frame 4, and later at rivet F3-5 at frame 3. Seven cracks were found at rivet F4-5, three were found at F3-5, and crack branching was observed at rivet F3-5 (Figure 6). The damage pattern at these three shear clip rivet holes was similar, with one faster-growing dominant crack and multiple smaller cracks. At 105,700 fatigue cycles, cracks were detected at rivet F2-5 at frame F2.

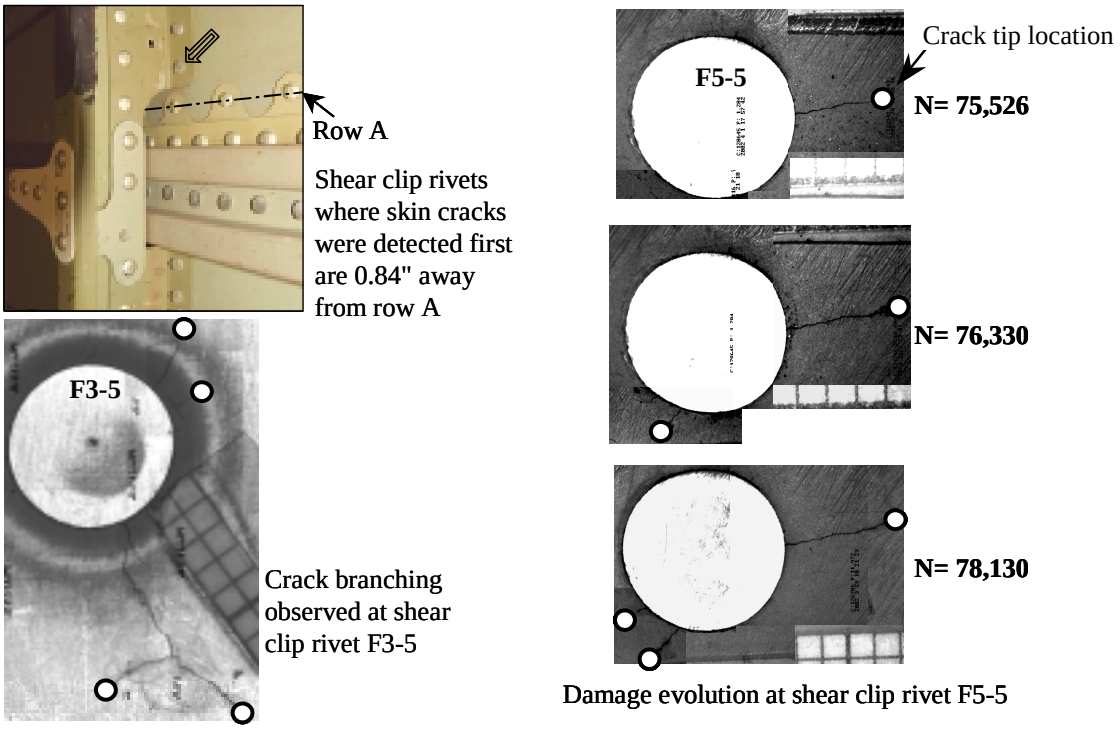

Figure 6. Damage growth at the shear clip rivets near the lap joint outer rivet row.

Figure 7 shows the MSD fatigue crack growth behavior in the test panel. The first four cracks detected in the lap joint (cracks A22L, A22R, A23L, and A23R) have similar growth behavior. The two

shear clip cracks, designated F3-5D and F5-5L, were detected earlier but grew slower compared to the cracks in the outer rivet row of the lap joint. This is a result of the higher stiffness at the shear clip attachment to the skin. Across a skin bay, the frame locations have the lowest hoop strain.

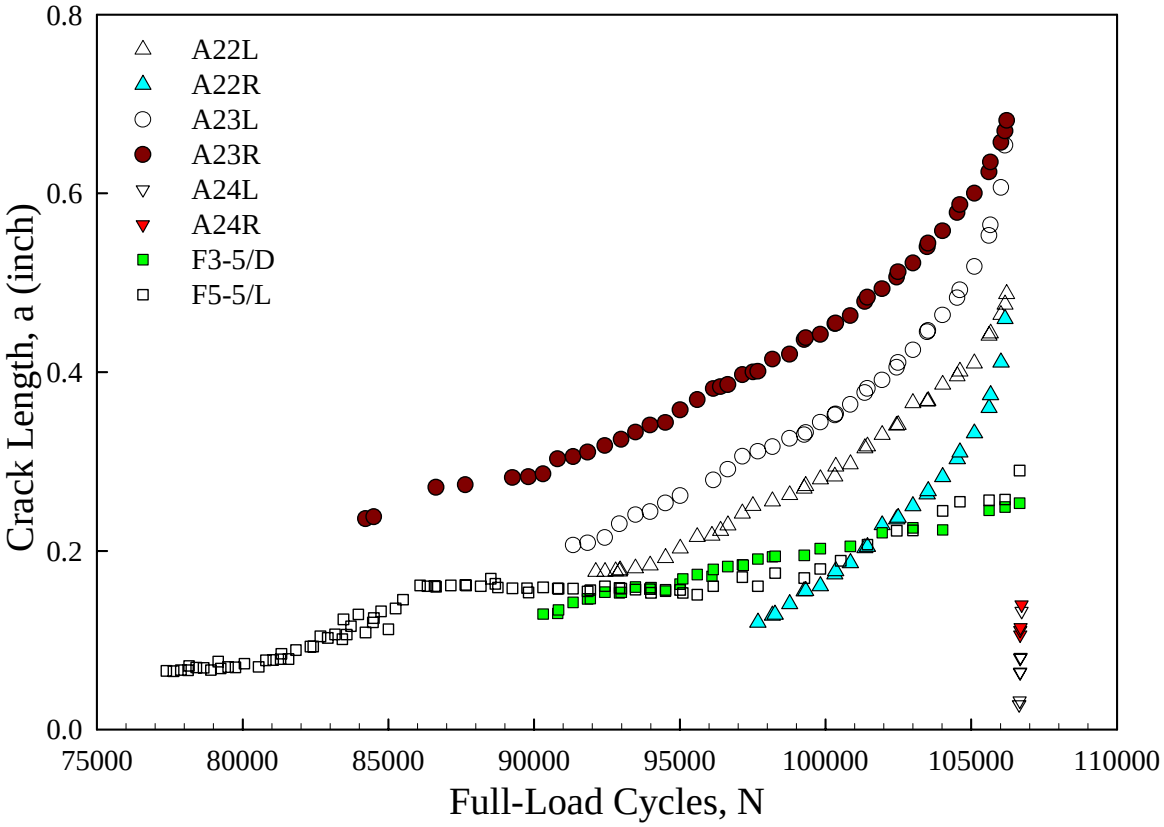

Figure 7. Crack size vs load cycles for cracks detected in the panel.

TRACLIFE was used to conduct probabilistic crack growth analyses of individual MSD cracks in the test panel prior to linkup. Figure 8 show TRACLIFE results for cracks A22L and A22R. TRACLIFE prediction was in good agreement with experimental results of crack A22L, but was on the conservative side for crack A22R. This crack was growing toward crack A23L and ultimately linked up with it. Similar TRACLIFE results were obtained for the two cracks at rivet A23.

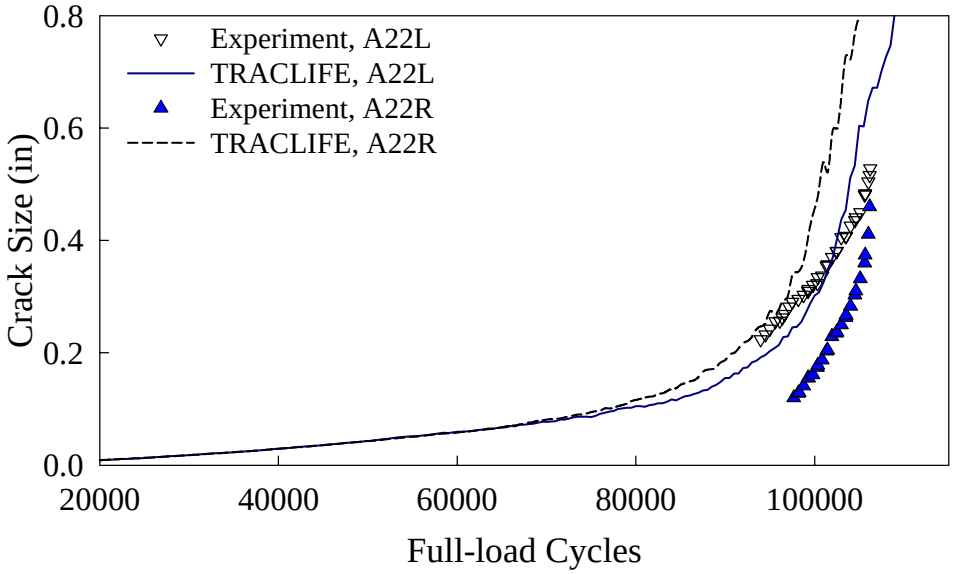

Figure 8. TRACLIFE analysis results for cracks at rivet A22.

(c) MSD Linkup

Figure 9 shows the first linkup of MSD cracks. It occurred after 106,217 full-load fatigue cycles in the outer rivet row of the lap joint between rivets A22 and A23. After the linkup, the lead crack had a total length of 2.87″. Figure 10 shows the different stages of growth of the lead crack formed by the first MSD linkup. Shortly after the first linkup, cracks were detected emanating from rivet hole A24. Cracks A24L and A24R were detected at cycles 106,644 and 106,680, respectively. Unlike the cracks at A22 and A23, the two cracks at A24 were completely linked to the rivet hole when first detected. Because of the high stress field created ahead of the lead crack, cracks A24L and A24R grew faster compared to the lap joint cracks detected earlier (Figure 7).

The second linkup happened 713 cycles after the first one when the lead crack and crack A24L bypassed each other. The two cracks slowed down and curved toward each other to form a football shape. After another 109 cycles (at 108,039 fatigue cycles), the lead crack grew into rivet hole A21 to the left. No crack was detected at rivet hole A21 before the linkup.

The lead crack then grew rapidly at both ends. At 107,425 fatigue cycles, the lead crack extended to the right through rivet hole A26 and linked up to one of the existing cracks at shear clip rivet F3-5. Shortly after that, a short crack was detected on the left side of rivet hole A27. By 107,458 cycles, the lead crack had grown to a total length of 16.04″, spanning slightly beyond rivet A27 to the right to about midway between rivets A16 and A17 to the left (Figure 10). At that point, the crack grew appreciably with every fatigue cycle and the fatigue test was terminated.

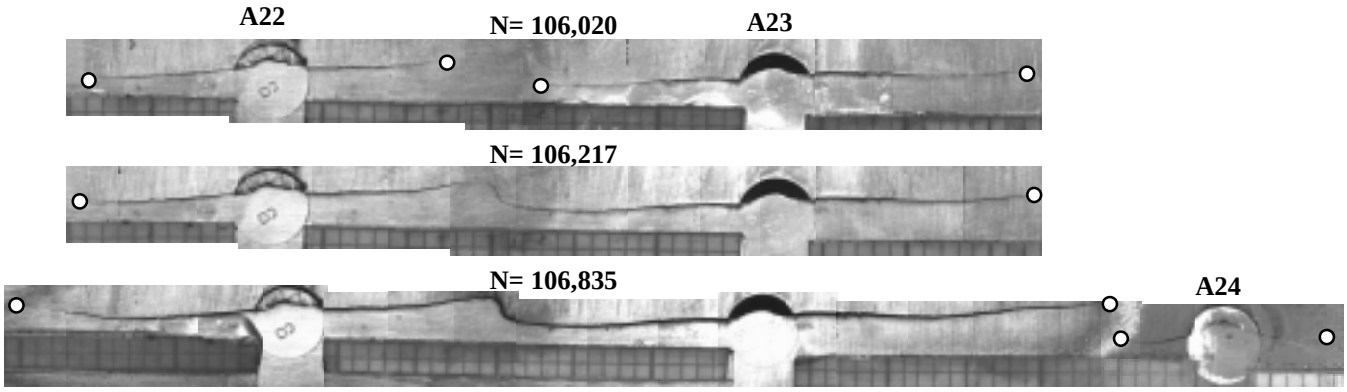

Figure 9. First MSD linkup occurred between rivets A22 and A23 in the lap joint outer rivet row after 106,217 full-load cycles.

Figure 11 shows the growth of the lead crack as a function of fatigue cycles up to the end of fatigue test at 107,458 cycles. The left and right crack lengths are measured from the centerline midway between rivets A22 and A23 where the first linkup occurred. It can be seen that the lead crack initially grew at approximately the same rate in both directions, but the growth rate of the right crack tip decreased significantly as it approaches frame F3. At the end of fatigue test the lead crack grew to a length of 16.04″, extending along the outer rivet row of the lap joint mainly in bay two but crossing over frame F3 slightly into bay three.

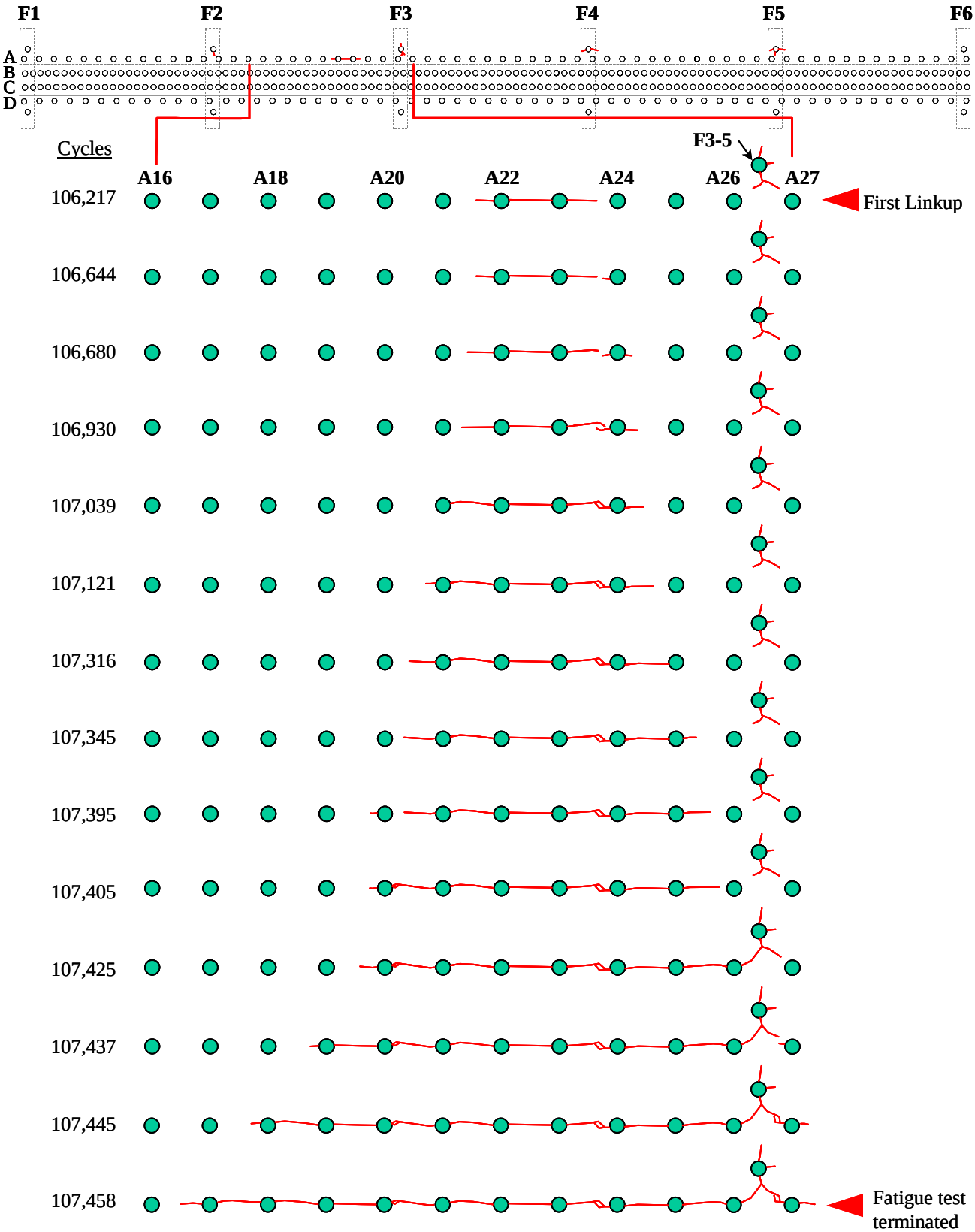

Figure 10. A schematic illustrating lead crack growth during the fatigue test

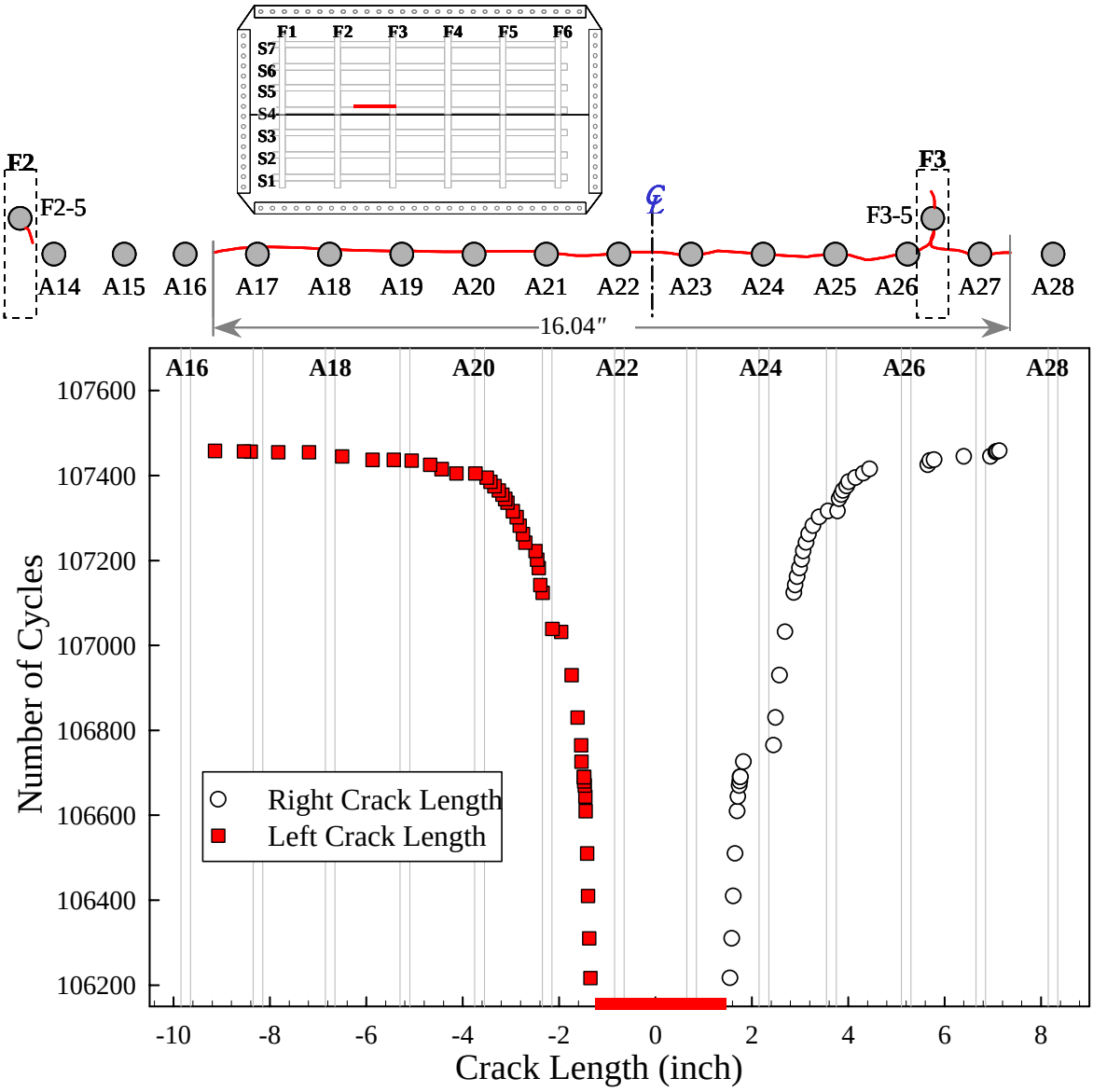

Figure 11. Growth of the right and left crack tips of the lead crack during the fatigue test.

In the finite element analysis of the lead crack formed by the first MSD linkup, the MCCI method was used to calculate the stress-intensity factors at the left and right crack tips. Figure 12 shows the relative weight of the stress-intensity factors in this mixed-mode crack growth scenario. ΔK_I (in-plane tension mode) amounts to about 80% of the total ΔK at each crack tip. Next in significance was Δk_2 (out-of-plane shear mode) representing about 19% of the total ΔK. The two remaining components, ΔK_{II} (in-plane shear mode) and Δk_1 (symmetric bending mode), were negligible. Noticeable skin bulging at the crack confirmed the relatively high Δk_2. The value of ΔK_I at the left crack tip was about 5% higher than that of the right crack tip. This difference in the dominant stress-intensity factor is attributed to the difference in the stress field. The difference in stress-intensity factors caused the asymmetric growth of the lead crack (Figure 11).

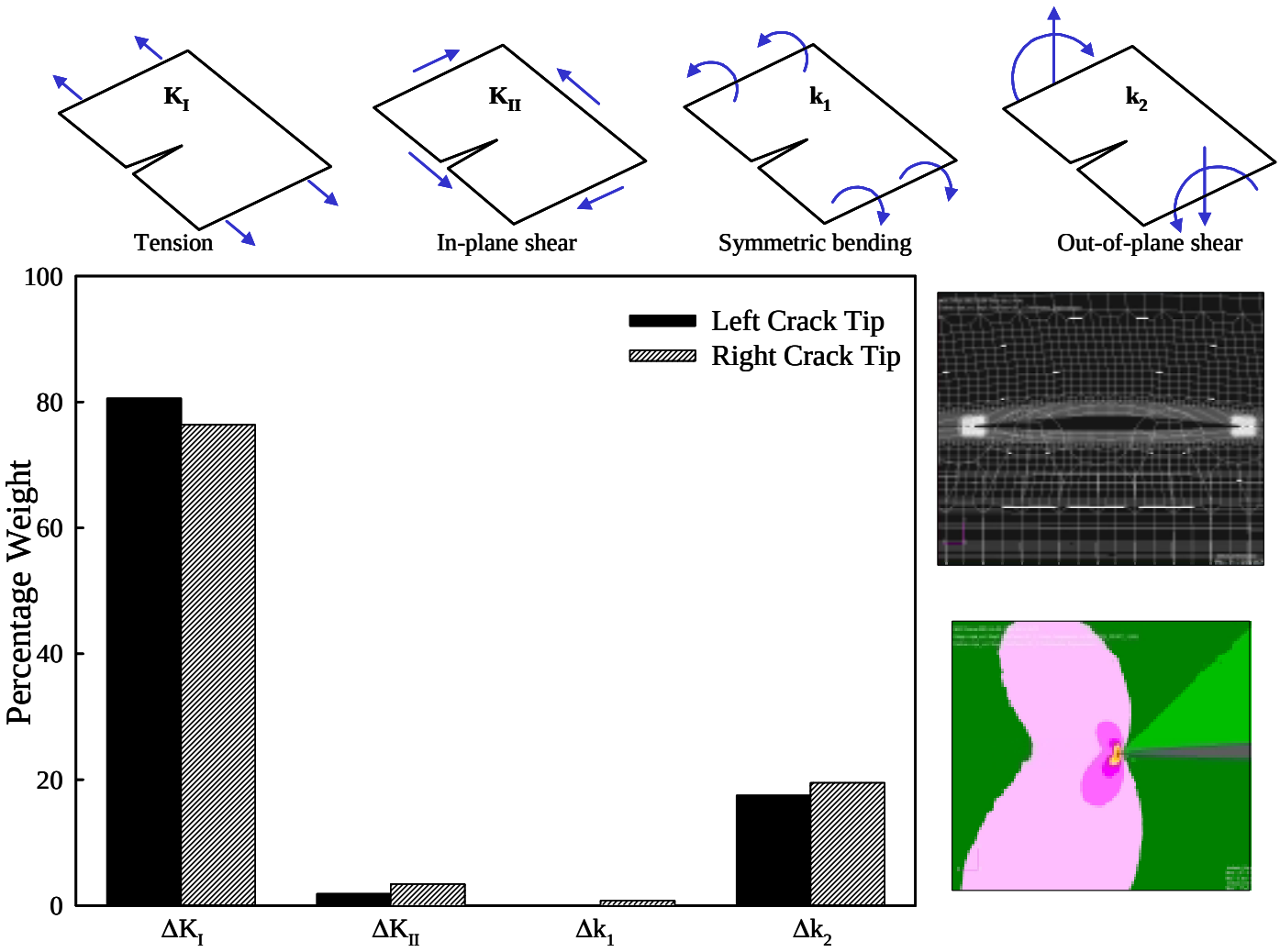

Figure 12. Relative weight of the stress-intensity factors at the crack tips of the lead crack.

Phase III, Residual Strength Test

During the residual strength test, loads were applied quasi-statically with a pressure increment of 2 psi up to 14 psi and an increment of 1 psi afterwards. Further crack extension was observed at 16-psi pressure. Catastrophic failure occurred at pressure 17.8 psi. The lead crack abruptly extended to a five-bay, 75″ crack. Figure 13 shows the final state of damage after the residual strength test. The left crack tip of the lead crack extended to frame F2, linked up with the crack at shear clip rivet F2-5, and then stopped about 0.5″ past rivet F2-5. The right crack tip extended much further, stopped between rivets A62 and A63 just before frame F6. As the crack extended through frames F4 and F5, it turned upwards and linked up with the cracks emanating from shear clip rivets F4-5 and F5-5 and skipped two or three rivet holes in row A before turning downwards to continue extending along the rivet row. A posttest inspection on the inner surface of the panel showed that frames F3, F4, and F5 all fractured under the lap joint. The damage at frame F4 is shown in Figure 13.

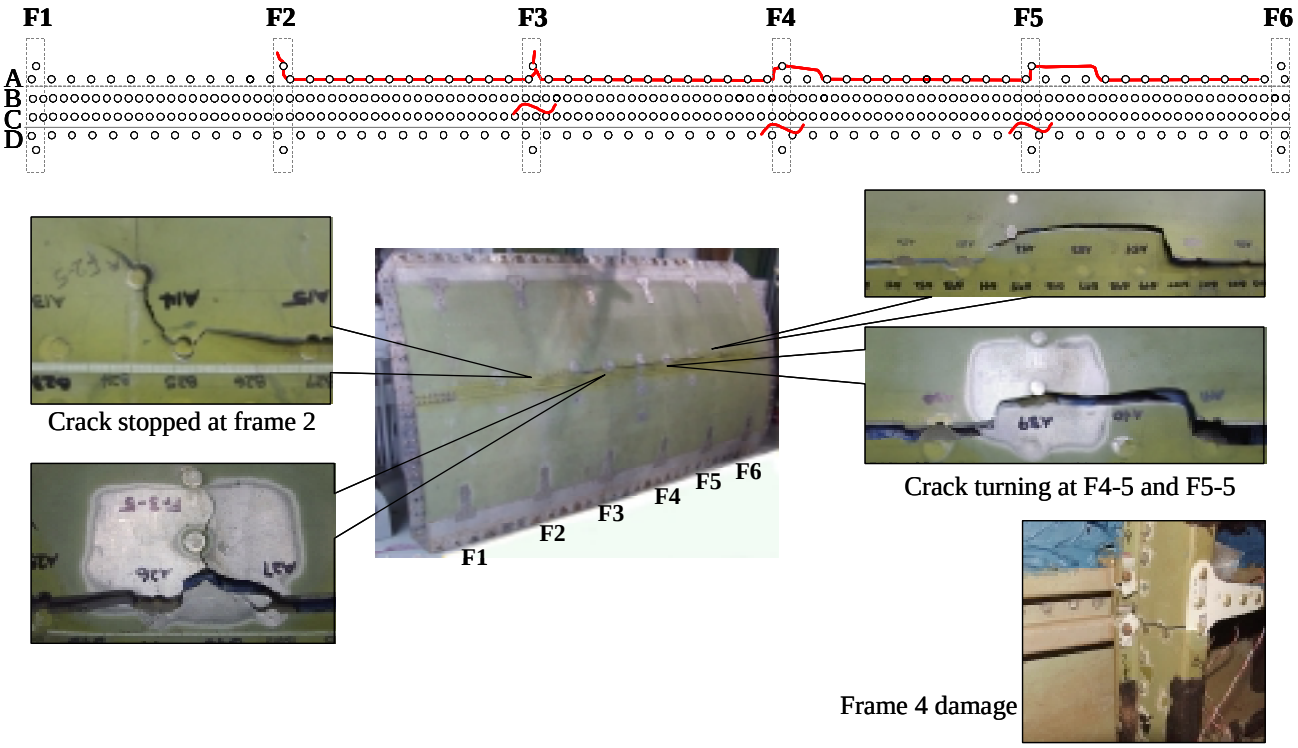

Figure 13. Final state of damage at the end of the residual strength test.

Concluding Remarks

Multiple-site damage initiation, growth, and interaction in an initially undamaged curved fuselage panel containing a longitudinal lap joint have been investigated. The panel was subjected to a constant-amplitude fatigue loading using the Full-Scale Aircraft Structural Test Evaluation and Research facility located at the Federal Aviation Administration (FAA) William J. Hughes Technical Center. Strain survey tests were conducted to ensure proper load introduction to the panel. During the fatigue test, rivets in the panel were periodically inspected for cracks using the Rotating Eddy-Current Probe system and the Remote-Controlled Crack Monitoring system. Cracks were initially found at the rivets that hold the shear clips to the upper skin near the lap joint. Faster-growing cracks were detected at rivets along the critical outer rivet row A of the lap joint. The first crack linkup occurred in rivet row A after 106,217 fatigue cycles, the lead crack then extended very rapidly and asymmetrically to a 16″, two-bay crack. The fatigue test was terminated when the crack grew with every fatigue cycle. A residual strength test was conducted with quasi-static loads to investigate the load-carrying capacity of the panel. Catastrophic failure occurred at a pressure of 17.8 psi. The lead crack extended instantaneously across five bays to a final length of 75″. Three frames were fractured under the lap joint. Fractographic analysis of the crack surfaces will be conducted to reconstruct crack growth histories.

A finite element model of the panel was developed and validated using quasi-static test results. The Modified Crack Closure Integral method was used to calculate the stress-intensity factors at the tips of the lead crack. The analysis showed that the opening-mode stress-intensity factor was the dominant mode. Finite element analyses will be continued to fully characterize fatigue crack growth in the curved panel. The FAA-sponsored risk assessment program, TRACLIFE, was used to conduct probabilistic analysis of crack growth behavior up to the first linkup for cracks detected in the lap joint outer rivet row. Good agreement was found between TRACLIFE predictions and the experimental results. Further probabilistic analyses of multiple cracks in the curved panel will be conducted.

Acknowledgement

The first and the last three authors would like to express their sincere appreciation to the FAA William J. Hughes Technical Center for its support through the FAA-Drexel Fellowship Research Grant (97-G-032) to Drexel University.

REFERENCES

1. J. McGuire and J. Foucault; 1999; Recommendations for Regulatory Action to Prevent Widespread Fatigue Damage in the Commercial Airplane Fleet; Final Report of the Airworthiness Assurance Working Group.
2. J. G. Bakuckas, Jr.; 2002; Full-Scale Testing and Analysis of Fuselage Structure Containing Multiple Cracks; DOT/FAA/AR-01/46.
3. B. Wincheski, J. Simpson, and R. Todhunter; 1997; A New Instrument for the Detection of Fatigue Cracks Under Airframe Rivets; *Review of Progress in Quantitative NDE*; Vol. 16B; pp. 2113-2121.
4. A. A. Ahmed, J.G. Bakuckas, Jr., C. A. Bigelow, P. Tan, J. Awerbuch, A. Lau, and T. Tan; 2002; Initiation and Distribution of Multiple-Site Damage (MSD) in a Fuselage Lap Joint Curved Panel; *Proceedings of the 6th Aging Aircraft Conference*; San Francisco, CA.
5. R. Kurth, F. Brust, N.D. Ghadiali, J. G. Bakuckas, Jr., and P. Tan; 2002; Damage Initiation and Residual Strength Modeling in Aircraft Structures and Comparison to Experimental Test Results from FASTER; *Proceedings of the 6th Aging Aircraft Conference*; San Francisco, CA.
6. S. A. Fawaz; 2000; Equivalent Initial Flaw Size Testing and Analysis; AFRL-VA-WP-TR-2000-3024.